Contract No:

This document was prepared in conjunction with work accomplished under Contract No. DE-AC09-08SR22470 with the U.S. Department of Energy (DOE) Office of Environmental Management (EM).

Disclaimer:

Characterization of Ceramic Material Produced from a Cold Crucible Induction Melter Test

Fuel Cycle Research & Development

Prepared for
U.S. Department of Energy Office of Nuclear Energy
Materials Recovery and Waste Forms Development Campaign

J.W. Amoroso and J.C. Marra
Savannah River National Laboratory

April 30, 2015

FCRD-MRWFD-2015-000133 Rev. 0
SRNL-STI-2015-00188 Rev. 0

APPROVALS

AUTHORS:

J.W. Amoroso, SRNL Process Technology Programs Date

J.C. Marra, SRNL Materials Science and Technology Date

TECHNICAL REVIEW:

C. L. Crawford, SRNL Process Technology Programs, Reviewed per E7 2.60 Date

APPROVAL:

D. H. McGuire, Manager Date
SRNL Process Technology Programs

SUMMARY

This report summarizes the results from characterization of samples from a melt processed surrogate ceramic waste form. Completed in October of 2014, the first scaled proof of principle cold crucible induction melter (CCIM) test was conducted to process a Fe-hollandite-rich titanate ceramic for treatment of high level nuclear waste. X-ray diffraction, electron microscopy, inductively coupled plasma-atomic emission spectroscopy (and inductively coupled plasma-mass spectroscopy for Cs), and product consistency tests were used to characterize the CCIM material produced. Core samples at various radial locations from the center of the CCIM were taken. These samples were also sectioned and analyzed vertically. Together, the various samples were intended to provide an indication of the homogeneity throughout the CCIM with respect to phase assemblage, chemical composition, and chemical durability.

Characterization analyses confirmed that a crystalline ceramic with desirable phase assemblage was produced from a melt using a CCIM. Hollandite and zirconolite were identified in addition to possible highly-substituted pyrochlore and perovskite. Minor phases rich in Fe, Al, or Cs were also identified. Remarkably only minor differences were observed vertically or radially in the CCIM material with respect to chemical composition, phase assemblage, and durability. This recent CCIM test and the resulting characterization in conjunction with demonstrated compositional improvements support continuation of CCIM testing with an improved feed composition and improved melter system.

CONTENTS

FIGURES

TABLES

ABBREVIATIONS

ANOVA	analysis of variance
ARM	approved reference material
At. %	atom percent
CCIM	cold crucible induction melter
C_i	concentration of element "*i*"
EA	environmental assessment
EDS	energy dispersive spectroscopy
EDX	energy-dispersive x-ray spectroscopy
f_i	fraction of element "*i*"
g	gram(s)
ICP-AES	inductively coupled plasma-atomic emission spectroscopy
ICP-MS	inductively coupled plasma-mass spectroscopy
INL	Idaho National Laboratory
k	kilo
K	Kelvin
LM	lithium-metaborate fusion
LRM	low-activity reference material
min	minute
NL_i	normalized element "*i*" release
PCT	product consistency test
PDF	powder diffraction file
PF	sodium peroxide fusion
RF	radio frequency
SA	surface area
SAED	selected area electron diffraction
SEM	scanning electron microscopy
SRNL	Savannah River National Laboratory
STEM	scanning transmission electron microscopy
T	temperature
TEM	transmission electron microscopy
V	volume
W	watt
Wt. %	weight percent
XRD	X-ray diffraction

ACKNOWLEDGEMENTS

The authors thank Phyllis Workman, Katie Hill, and David Missimer at Savannah River National Laboratory for assistance with sample preparation and property measurements. The authors thank Tommy Edwards at Savannah River National Laboratory for statistical analysis of certain data. The authors thank Vince Maio for useful technical discussions and expedient delivery of CCIM material. The authors thank Kyle Brinkman and Yun Xu at Clemson University for select SEM-EDS and XRD analysis. The authors thank Ming Tang at Los Alamos National Laboratory for TEM/STEM and EDX/SAED.

This work was supported by the U.S. Department of Energy, Office of Nuclear Energy, under Contract DE-AC02-06CH11357.

1 INTRODUCTION

Savannah River National Laboratory (SRNL) is developing melt-processed reference ceramic waste forms for treatment of waste streams generated by reprocessing commercial spent nuclear fuel. The waste form is designed to crystallize upon cooling from a melt (melt-processing) into a multiphase ceramic. Compositions are designed based on combinations of the waste and additives to target desired hollandite, perovskite, and pyrochlore phases. Elements with a +3 or +2 valance form perovskite ($(A^{+2})TiO_3$) and pyrochlore ($(A^{+3})_2Ti_2O_7$) type phases.[1,2] Zirconium (+4 valence) partitions to a zirconolite ($CaZrTi_2O_7$) phase.[3] Cs and Rb elements partition to a hollandite structure based on the general formula $Ba_xCs_yM_zTi^{+4}_{8-z}O_{16}$ where z = 2x+y for trivalent cations and z = x+y/2 for divalent cations for charge compensation.[4-6]

Idaho National Laboratory (INL) recently (October 2014) conducted a cold crucible induction melter (CCIM) test with a ceramic waste form (non-radioactive) developed at SRNL to demonstrate proof of principle for processing multi-phase crystalline waste forms from a melt. Prior to the CCIM testing, property data (e.g., high temperature viscosity and electrical conductivity) was collected for two potential test compositions. One, designated 'Fe-MP' was designed towards optimized processing and the other, designated 'CAF 5%TM MP' was designed towards optimized phase formation. The Fe-MP composition is an early developed composition that suffers from improper phase assemblage, but melts a relativey low composition and was expected to be adequate for processing in the CCIM as currently configured at INL. The CAF-5%TM-MP composition was formulated based on a baseline Cr/Al/Fe-based hollandite composition but with 5% addition of transition metal (TM) elements in an effort to enhance melt-ability for processing in the CCIM. The CAF-5%TM-MP composition forms more-desirable phases upon cooling but melts at temperatures that would test the limits of INL's CCIM as configured at the time.[7] It was recommended, and ultimately decided to perform initial CCIM testing using the Fe-MP composition with the intention to gather information regarding the performance of the melter, particularly with regard to processing a ceramic material (which had not yet been performed with INL's CCIM) to be used to support subsequent CCIM testing with more ideal feed compositions.

During this initial test, the drain operation could not be completed and instead of casting the ceramic into a mold, the melt was allowed to cool to room temperature in the melter. Subsequently, core samples were taken of the material remaining in the CCIM after cooling and characterized. Additionally, the drain assembly was analyzed to determine the extent of the drain operation during this test and the factors limiting a successful drain operation. The information presented in this report is intended to support future successful CCIM tests.

2 CCIM TEST SUMMARY[a]

INL personnel melted and attempted to pour a ceramic waste form composition using the CCIM. The feed material for the CCIM was supplied by Mo-Sci Corporation (Rolla, MO) as a dry stoichiometric mixture of oxide and carbonate reagents totaling ~30 kg. SRNL performed chemical analysis to confirm the feed material composition prior to use (Refer to Section 3.1.2). The targeted and measured elemental and feed chemical concentrations are listed in Table 1. In general, the prepared feed measured composition was within typical analytical uncertainty of the target composition.

Table 1. Target and Measured Elemental Concentrations (wt. %) in CCIM Feed Material.

	Target	Measured
Ba	10.69	10.25
Ca	0.93	0.91
Cd	0.09	0.04
Ce	2.48	2.43
Cs	2.54	2.19
Eu	0.14	0.17
Fe	10.00	9.76
Gd	0.13	0.13
La	1.26	1.17
Mo	0.53	0.37
Nd	4.19	3.74
Pr	1.16	1.18
Rb	0.36	n.m.
Se	0.05	<0.10
Sm	0.87	0.90
Sn	0.05	0.09
Sr	0.78	1.01
Te	0.49	0.55
Ti	27.55	27.15
Y	0.46	0.44
Zr	2.07	1.98
Sum[b]	66.8	64.5

Batch Chemical	Target	Calculated
$BaCO_3$	15.36	14.72
$CaCO_3$	2.31	2.28
CdO	0.10	0.05
CeO_2	3.05	2.98
Cs_2CO_3	3.11	2.69
Eu_2O_3	0.16	0.19
Fe_2O_3	14.29	13.95
Gd_2O_3	0.15	0.15
La_2O_3	1.48	1.37
MoO_3	0.79	0.57
Nd_2O_3	4.89	4.37
Pr_6O_{11}	1.40	1.43
Rb_2CO_3	0.49	n.m.
SeO_2	0.08	<0.14
Sm_2O_3	1.01	1.04
SnO_2	0.07	0.11
$SrCO_3$	1.31	1.70
TeO_2	0.61	0.69
TiO_2	45.96	45.31
Y_2O_3	0.59	0.56
ZrO_2	2.79	2.68
Total	100.0	96.8

A Ti initiator ring and approximately 13.5 kg of feed material was packed into the CCIM. This initial charge was approximately 6 inches tall used for primary ignition of the melt. A full melt was achieved in approximately 3 hours at which point additional feed was added at 5.5 kg/hr. The CCIM's RF generator was operating at its maximum design power (60 kW) level to maintain the melt and after approximately 40 minutes and 3 kgs[c] of added feed an attempt was made to drain the melter. Nitrogen cooling to the

[a] The experimental parameters and operating conditions during the CCIM test are presented in greater detail elsewhere. (See V. C. Maio, "Production of a Low Temperature SYNROC All Ceramic Surrogate High Level Waste Form in INL's Cold Crucible Induction Melter Pilot –Validation of Test Completion," *U.S. Department of Energy Report INL/MIS-14-34012 (FCRD-SWF-2015-00256)*, Idaho National Laboratory, Idaho Falls, ID (2014).)

[b] Measured and calculated values do not include Rb contribution.

[c] Although the feed rate was continuous, the feeder was only run intermittently.

drain assembly was terminated and the drain tube heater was turned on. The heater burnt out in less than five minutes of being turned on. In an attempt to utilize as much latent heat as possible, cooling water to the drain system was decreased, but the system was unable to sustain the lower cooling rate and a leak in the cooling system (presumably from boiling water) triggered the automatic shutdown of the RF generator and termination of the test.

Additional cooling was supplied to the crucible stays in an attempt to increase the temperature gradient across the crucible during cooling so that samples could be subsequently taken having undergone different cooling rates. The estimated cooling time for the center of the melt was approximately 4 hours, or ~ averaged 6 K/min. Obviously, the outer material cooled faster and the water cooled crucible walls could have realistically generated cooling rates in the 100's K/min range. Seven core samples were taken from the solidified melter material and characterized. In addition, the drain assembly was removed and characterized. Preliminary characterization results and pertinent experimental procedures are presented subsequently.

3 CORE SAMPLES

3.1 Experimental

3.1.1 Sample Preparation

Seven 1-inch diameter core drilled samples were taken from the solidified material in the CCIM. The locations and depth dimensions for the core samples from the melter material are shown in Figure 1 and Table 2. Morphology differences along the vertical axes of the core samples were visually evident in the as-received core samples. In general, three morphologies were evident in each sample; dense, columnar, and porous. These regions were designated Zone 1, Zone 2, and Zone 3, respectively. As many of the cores cracked during drilling, the cores were appropriately reassembled (temporarily held together with super glue) prior to characterization in order to link subsequent results to different areas within each core. Digital images representative of the as-received and cross-sectioned core samples are shown in Figure 2 and Figure 3, respectively.

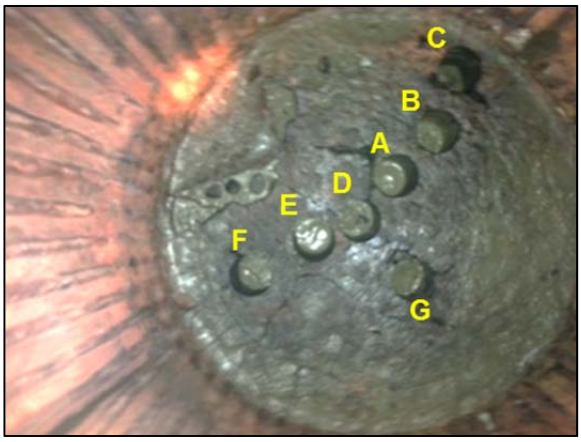

Figure 1. Digital image of solidified material in melter showing core sample locations.

Table 2. Core sample dimensions.

Core	Core Depth (inch)
A	1 3/8
B	1 1/2
C	1 11/16
D	1 3/8
E	2
F	1 5/8
G	1 1/4

Figure 2. Core sample F as-received after re-assembly.

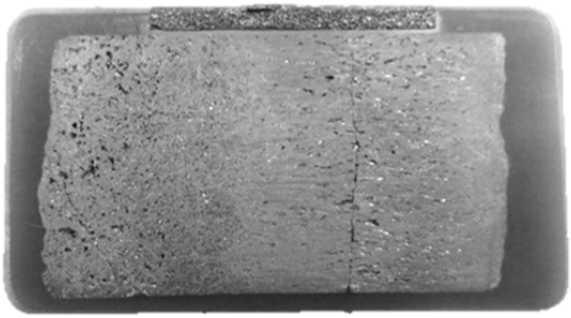

Figure 3. Core sample F cross-section mounted in epoxy.

3.1.2 Chemical Composition

Inductively Coupled Plasma-Mass Spectroscopy (ICP-MS) was used to measure Cs concentrations and Inductively Coupled Plasma-Atomic Emission Spectroscopy (ICP-AES) was used to measure all other elemental concentrations as Cs cannot be measured by ICP-AES. A representative amount from each sample was prepared via a sodium peroxide fusion (PF) method and a lithium-metaborate fusion (LM) method. Both digestions methods were used because the high concentrations of TiO_2 and Cr_2O_3 are difficult to fully dissolve with the LM fusion method (the preferred digestion for low concentration analysis). Digested samples were analyzed in duplicate for each element of interest by ICP-AES for a total of 4 measurements per element. Cs analysis was only measured in duplicate from the PF digestion solutions. The instrumentation was re-calibrated between the duplicate analyses and standards were intermittently measured to ensure the performance of the ICP instruments over the course of the analyses. The measured cation concentrations were converted to their respective oxide to obtain a wt. % of each component oxide.

3.1.3 Fe RedOx

The Fe^{2+}/Fe^{3+} and Fe^{2+}/Fe (total) ratios were determined from an absorption method using a UV-Vis spectrometer. Samples were dissolved in a sulfuric-hydrofluoric acid mixture, containing ammonium vanadate to preserve the Fe^{2+} content. Boric acid was added to destroy iron-fluoride complexes and ferrozine was added to form ferrous-ferrozine complexes for the determination of Fe^{2+} content. An additional measurement with ascorbic acid addition to reduce Fe^{3+} to Fe^{2+} with a second absorbance measurement was used to determine total Fe.[8]

3.1.4 Phase Identification and Microstructure

Samples were characterized with x-ray diffraction (XRD, D8 Advance, Bruker AXS Inc., Madison, WI) to identify the resulting phase(s). Portions of each sample were initially ground in an automatic Spex mill for 4 minutes with agate cup and media. Subsequently, the powders were hand ground with an agate mortar and pestle in alcohol and mounted to a glass slide using a collodion/Amyl Acetate solution. The XRD patterns were collected at a 0.02° stepped scan from 5 – 70 ° 2θ at a scan rate of 1 sec/step. Complementary XRD patterns were collected from 10 – 70 ° 2θ at a scan rate of 1 °/min (Rigaku D/Max 2100 Powder X-ray Diffractometer) and the patterns were refined using the Jade Software package to estimate phase abundances.

Scanning Electron Microscopy (SEM) and Energy Dispersive Spectroscopy (EDS) measurements were performed at the Advanced Materials Research Lab at Clemson University with a Hitachi -SU6600 SEM. EDS mapping of Cs, Ba, Mo, Zr, Cr, Al, Fe, Nd, Ca, La, Ce, and Ti was performed. Complementary imaging and EDS was performed at SRNL with a Hitachi TM3000 SEM.

Transmission electron microscopy (TEM)/scanning transmission electron microscopy (STEM)/ Energy-dispersive X-ray spectroscopy (EDX) was performed using a FEI Tecnai F30 electron microscope, operating at 300 kV. Samples were thinned to below 10 µm in thickness by mechanical polishing, then to electron transparent (less than 200 nm in thickness) using a precision ion polishing system (PIPS). EDX spectra were used to identify chemical composition of observed crystalline phases and selected area electron diffraction (SAED) patterns and high resolution TEM observations were used to determine the crystal structure of phases.

3.1.5 Chemical Durability

A crushed sample leaching test (Product Consistency Test (PCT) Method-A) was performed in triplicate on each sample to assess aqueous chemical durability.[d] Also included in the experimental test matrix was the Environmental Assessment (EA) benchmark glass,[9] the Approved Reference Material (ARM), the Low-activity Reference Material (LRM), and blanks from the sample cleaning batch. All standards were ground, washed, and prepared according to the standard PCT procedure.[10] Fifteen milliliters of water were added to 1.5 g of sample or standard in stainless steel vessels. The vessels were closed, sealed, and placed in an oven at 90 ± 2 °C where the samples were maintained at temperature for 7 days. Once cooled, the resulting solutions were sampled (filtered and acidified), and analyzed. Samples of a multi-element, standard solution were also included as a check on the accuracy of the ICP-AES instrument used for these measurements. Normalized elemental release was calculated based on the target and measured compositions using the average of the common logarithms of the leachate concentrations according to the equation below,

$$Log\left[NL_i\right] = Log\left[\frac{C_i \cdot (sample)}{f_i \cdot SA/V}\right]$$

where C_i is the concentration of element "*i*" (e.g., Cs) in solution (g/L), f_i is the fraction of element "*i*" in the unleached sample[e] (unitless), SA is the surface area of the sample (m^2), and V is the volume of leachant solution (L) resulting in a normalized element "*i*" release (NL_i) having units of g/m^2. The NL_is were normalized to one to compute a unit less figure of merit for each elements release. This methodology is used as method to compare relative release between samples and is not intended to quantify or predict long term durability of ceramic materials in aqueous environments.

3.2 Results & Discussion

3.2.1 Chemical Composition

Samples were selectively chosen for chemical analysis and grouped according to visual morphology (refer to 3.1.1 for discussion of morphology). Figure 4 is images of a representative core (sample F) in which dense, columnar, and porous morphologies are evident along the length of the core. In general, it was straight-forward to identify and section samples that were either dense or columnar in appearance. Such samples were labeled *Zone 1* and *Zone 2* respectively. It was more difficult to accurately identify porous sections due to a less definitive transition from the columnar morphology to the porous morphology. Therefore, samples that could be identified as porous were sampled and labeled as *Zone 3*. A fourth set of samples consisting of Zone 2 and Zone 3 material where a definitive distinction was

[d] The PCT has been used in the melt-processed ceramic development effort as a convenient method to measure specific elemental releases to identify phases with low durability. For example, the test has identified that a Cs-Mo phase found in some non-optimized formulations resulted in high elemental releases of Cs and Mo. At this time, the test is not being used to provide quantitative durability values.

[e] In all cases, measured elemental concentrations were used as opposed to target concentrations.

difficult to identify were measured and labeled *Zone 5*. One additional sample was measured that was not sectioned prior to analysis, representing the bulk material. In total, 29 samples taken from 4 different cores and from various (~7) bulk regions in the melted CCIM material were analyzed.

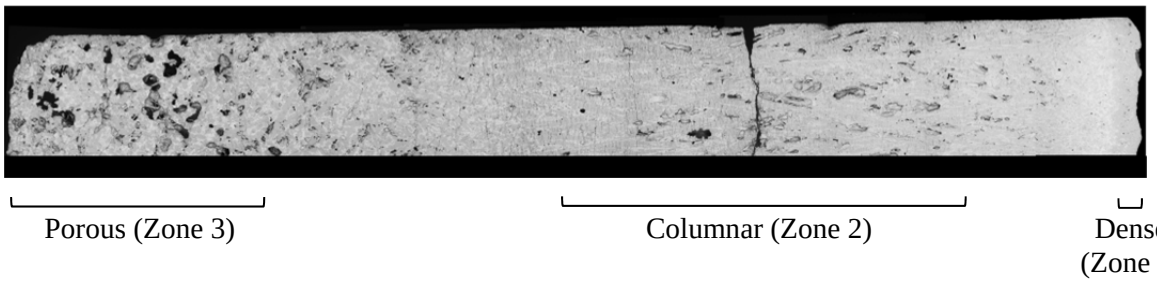

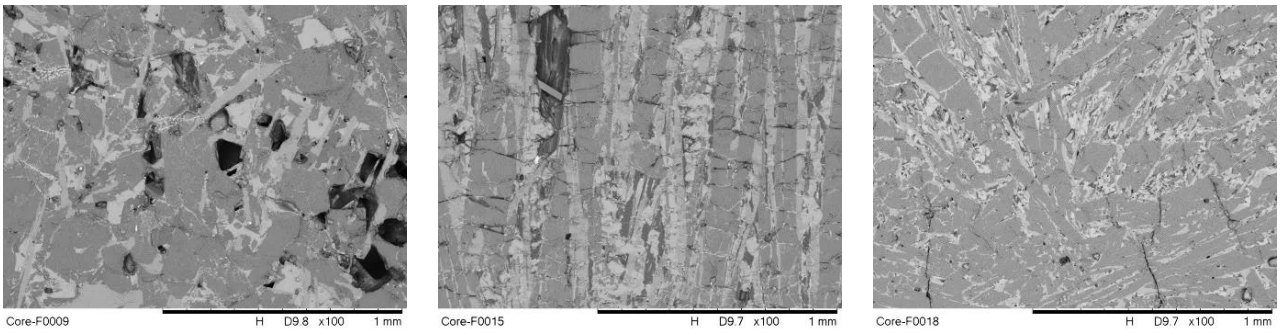

Figure 4. SEM phase contrast images that reveal morphology differences along the length of the core sample.

Table 3 lists the measured elemental concentrations in the bulk CCIM material as represented by the sample that was not analyzed by zone. In general, the results indicate that the CCIM material composition was comparable to the target composition excepting Al, Cs, Mo, and Te. Although no Al was added to the CCIM feed material, these materials are known to readily react with available Al_2O_3. It is suspected that much of the Al from the crucible used to hold the initiator ring in place[f] reacted during the CCIM processing and additional Al may also have been introduced from refractory used in the CCIM. Cs is a highly volatile species and previous experiments have generally shown that about 50% of the Cs is lost during heating. However, in this CCIM test, it appears that less Cs was lost, about 32%.[g] Substantial amounts (>70%) of Mo and Te were unaccounted for in the measured analysis.[h] Whereas Cs is known to volatilize, Mo and Te are not known to volatilize at such rates that would explain the results. Ultimately, the fate of the Mo and Te are unknown.

[f] Refer to reference in footnote a for a discussion of the initiator ring setup.
[g] Table 1 indicates the feed material could have been deficient in Cs and Mo by as much as ~15% and ~30%, respectively. Therefore, the Cs (and Mo) retention would be greater than if calculated from Table 3.

Table 3. Measured elemental concentrations (wt. %) in the bulk CCIM sample that was not analyzed by zone.

Element	Target	Measured
Al	0.00	2.21
Ba	10.69	10.54
Ca	0.93	0.93
Cd	0.09	<0.10
Ce	2.48	2.47
Cs	2.54	1.73
Eu	0.14	0.12
Fe	10.00	9.88
Gd	0.13	0.12
La	1.26	1.22
Mo	0.53	0.15
Nd	4.19	4.02
Pr	1.16	1.21
Rb	0.36	n.m.
Se	0.05	<0.10
Zr	2.07	1.97
Sm	0.87	0.85
Sn	0.05	n.m.
Sr	0.78	0.99
Te	0.49	0.13
Ti	27.55	30.13
Y	0.46	0.40

Chemical composition was also measured as a function of Zone and radial location. Figure 5 shows the measured elemental concentration means for each Zone with corresponding standard error bars. In general, chemical composition did not appear to depend on the zone from which the material came, indicating that the CCIM material was relatively homogeneous. However, the data shown in Figure 5 do appear to indicate greater variation in the means of the measured values for Al[i] and the lanthanide series elements. Analysis of variance (ANOVA) was used to test for statistically significant differences in the data between zones. The results of the ANOVA indicated statistically significant differences (at the 5% significance level) for Ce, La, Nd, Pr, Sr, and Te. Specifically, the means for Ce, La, and Pr were not statistically significant between zones 1, 2, and 5, or between zones 3 and 5 (i.e. Zone 5 is common). Similarly, the means for Nd and Sr were not statistically significant between zones 1, 2, and 5 or between zones 2, 3, and 5 (i.e. zone 2 and 5 are common). The means for Te were not statistically significant between zones 1, 3, and 5 and there was no common connection to zone 2.

[i] The variance in the Al concentration is unknown.. However, closed-end Al_2O_3 cylinders were used to support a Ti initiator ring during processing that were observed to significantly react with the feed material as evidenced by one of the supports having been found to be significantly dissolved compared to its initial dimensions.. It is possible that some samples were taken nearer those Al_2O_3 supports than other samples and thus would have relatively increased Al concentration.

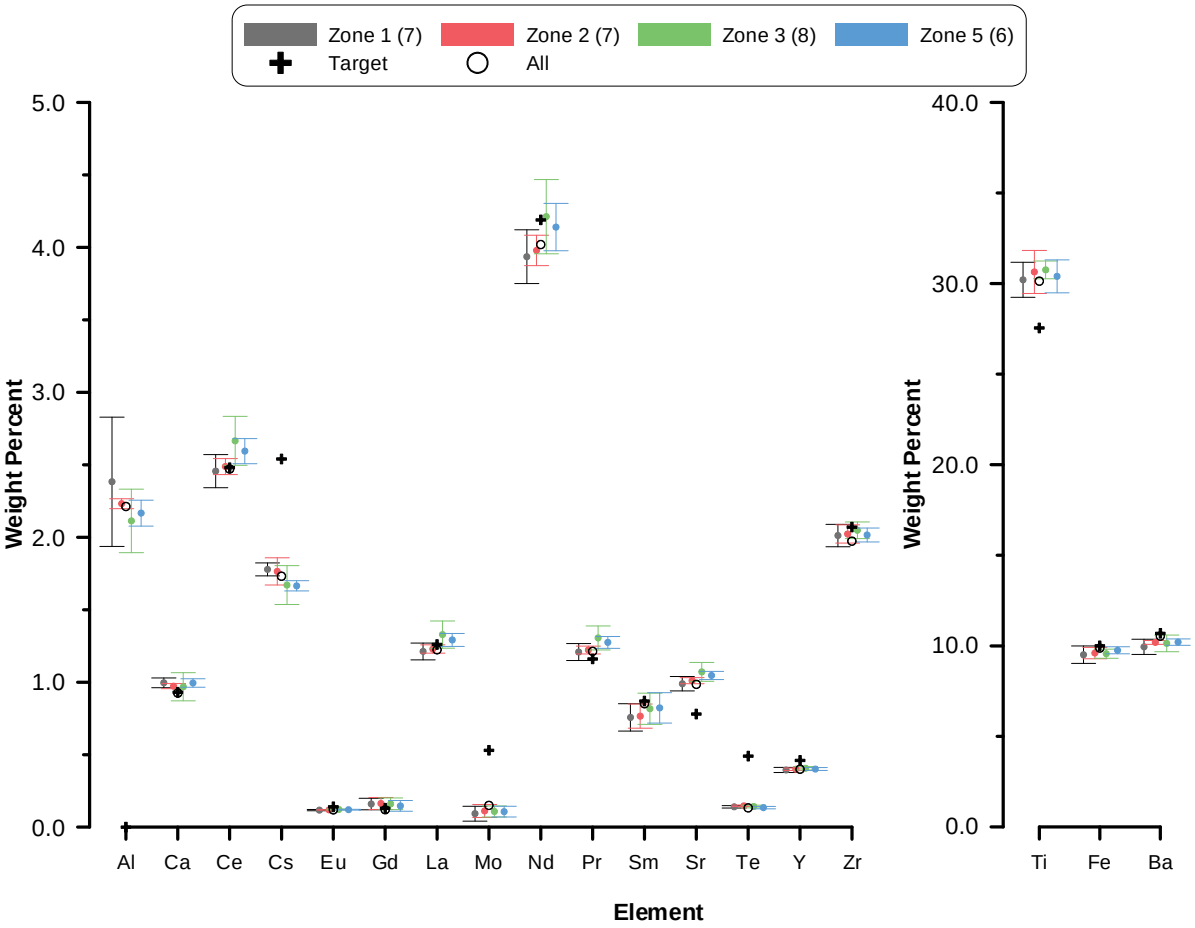

Figure 5. Plot of mean elemental concentrations and corresponding standard deviation from samples grouped according to morphology (Zone) type.

In practical terms, the ANOVA results, the subjectivity involved with differentiating distinct boundaries between zones (morphology transitions, in particular between zone 3 and 2, hence the use of zone 5), and the microscopy results (Section 3.2.3) indicate most lanthanide series elements are likely distributed less uniformly than other elements. Nevertheless, the magnitude of those differences remains small; the elemental variances shown in Figure 5 are typically less than 0.5 wt. %.

Figure 6 shows the same composition data as that shown in Figure 5 except the data is grouped according to core sample, or radial position from the center of the melter. In general, smaller standard errors (relative to the Zone analysis) were observed across cores excepting core F, which exhibited the greatest variation. The variation in Core F measurements is attributed to Zone 3 measurements in which many of the lanthanide series elements were the greatest of all the samples in the study.[j] This result further supports the previous conclusion that lanthanide series elements were distributed less homogeneously than other elements, particularly in the porous regions of the CCIM ceramic material. Given that Core F was also located near the edge of the crucible, it is possible that cooling differences or interactions with the cold wall of the melter may influence elemental partitioning. Overall, the chemical composition measurements were remarkably consistent. The data confirms that the CCIM mixes the melt very well and demonstrates the melt was homogenous both radially and vertically.

[j] Additional statistical analysis was performed to determine the impact of Core F Zone 3 measurements on the ANOVA results of the Zone grouping. Core F Zone 3 was not found to bias the previous conclusions.

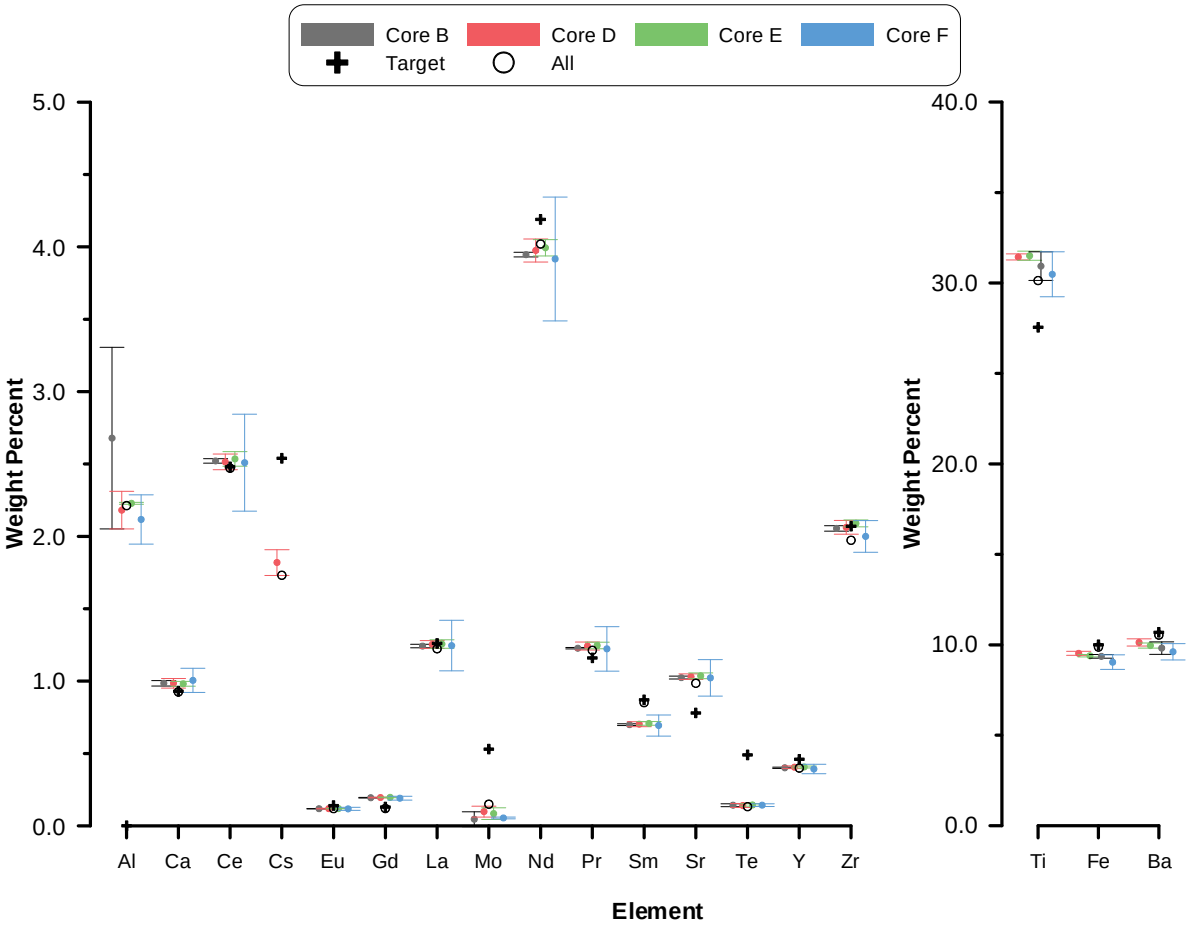

Figure 6. Plot of mean elemental concentrations and corresponding standard deviation from samples grouped according to radial distance. (D: center, E: ½ radius, F: edge, B: ½ radius)

3.2.2 Fe RedOx

The redox state is of interest because reduced melts are known to have positive effects on the final properties of the ceramic.[11,12] Ti metal was added to the CCIM during initiation and it was expected that some amount of reduction was possible. Fe redox was measured on one sample, Core D, to determine the redox of the CCIM material. As with the other analyses, Fe redox was measured for different zones (morphology) within the core. The results, summarized in Table 4, indicated that the CCIM material was partially reduced (~20% Fe^{2+}).

Table 4. Measured Fe^{2+} Fraction in Core D

	Fe^{2+} / Fe Total
Zone 1	0.13
Zone 2	0.19
Zone 3	0.24
Zone 5	0.20

3.2.3 Microstructure and Phase Analysis

XRD confirmed three primary phases in the core samples as hollandite, pyrochlore, and zirconolite. Phase analysis conducted on the different morphologies observed in the individual cores indicated similar phase assemblage. In general, the XRD results indicate material in the CCIM was homogenous varying depths in the melt as well as radially from the center to the edge of the melt. XRD patterns for three cores positioned radially from the center of the melter are shown in Figure 7 and calculated phase abundances calculated from the XRD patterns is summarized in Figure 8. Included in Figure 8 is the estimated phase abundance based on the target composition and normalized for the three measured primary phases. In general, the estimated and measured phase information indicates the CCIM test was successful in producing a homogenous ceramic from a melt.

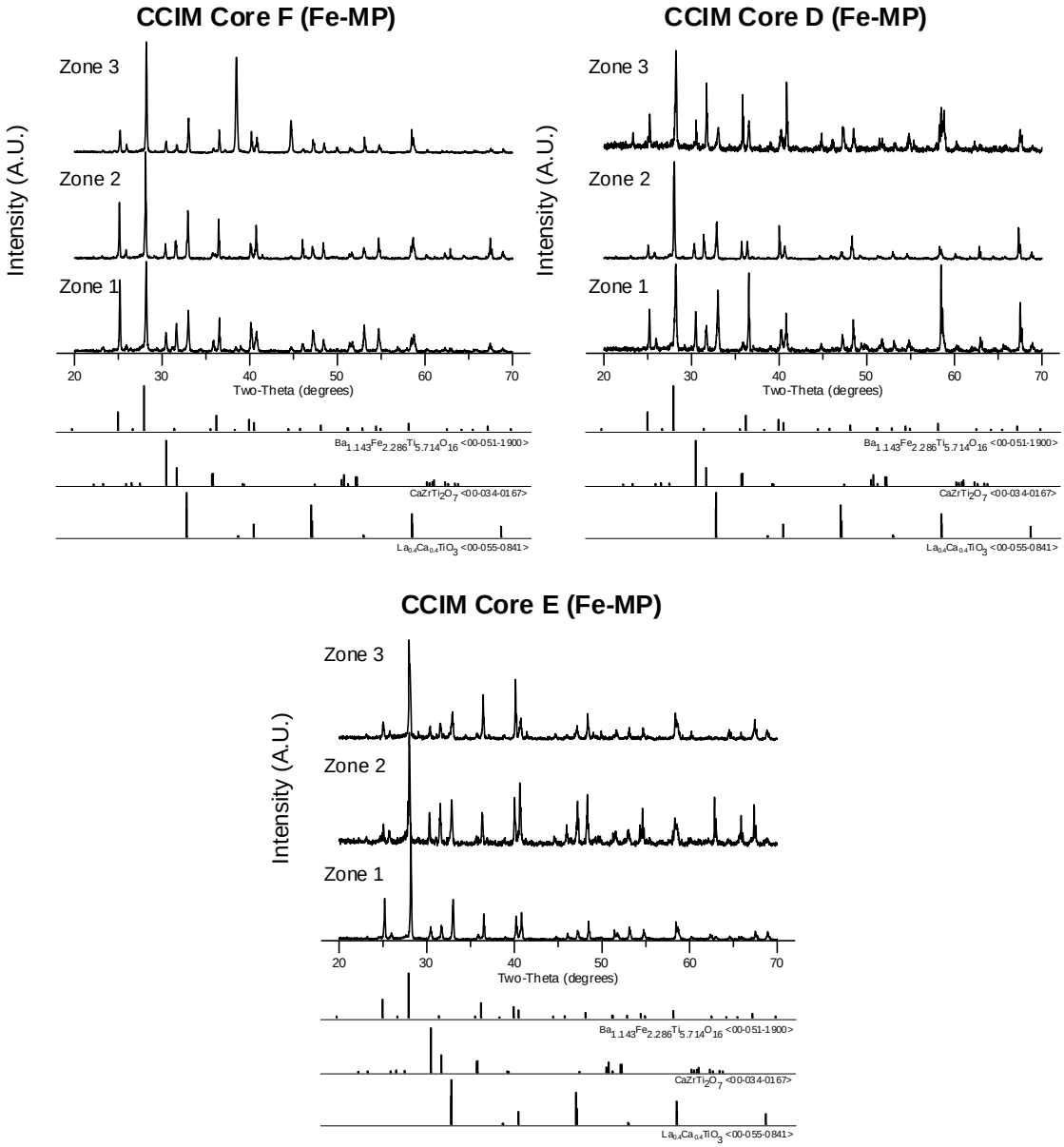

Figure 7. XRD patterns of Core E sample sections. Labeled patterns: Z1 = dense material, Z2 = columnar material, and Z3 = porous material.

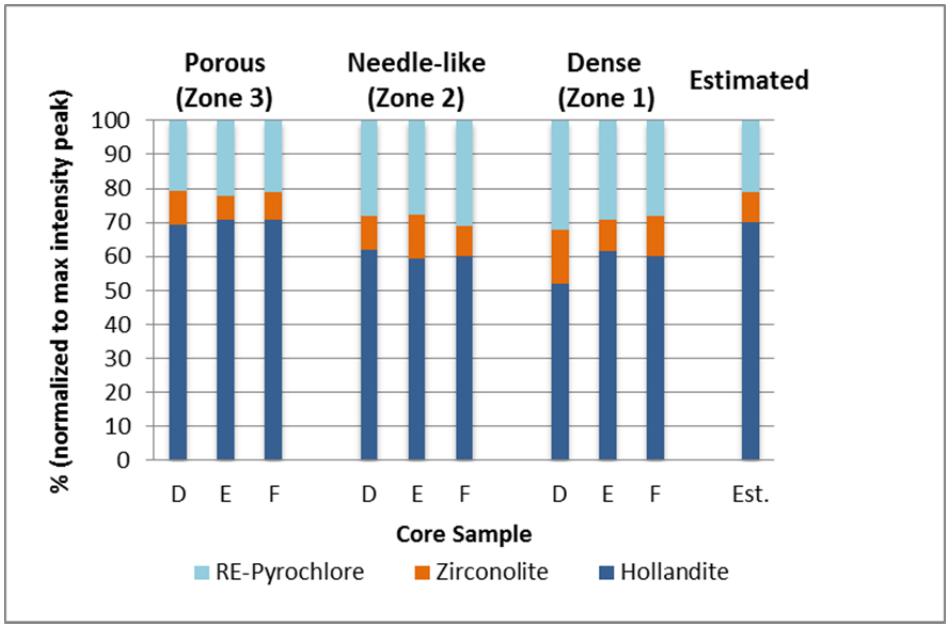

Figure 8. Summary of primary phase abundances in core samples compared to estimated abundances based on feed composition and target phase assemblage.

SEM images and corresponding EDS elemental maps of areas from Core D Zone 1 (dense), 2 (columnar), and 3 (porous) are shown in Figures 9 – 11. In all SEM images, 3 – 5 contrast phases are visually evident and no significant differences in elemental partitioning are visually evident in the maps, as expected based on chemical composition and XRD analyses. Semi-quantitative elemental analysis was performed on several samples resulting in similar chemical makeup for the various phases. Representative EDS semi-quantitative elemental[k] compositions are shown in Table 5 – Table 7. In those tables, phases were identified based on the elements listed in bold type (those that measured greater than 1 atom %). Notably, the hollandite phase contains Al, which is known to readily substitute into hollandite structures and is used to stabilize pure Fe-hollandite ceramics.[5,6,11] Hollandite is most distinctly identified in the Ba and Ti maps. Pyrochlore/perovkite and zirconolite phases identified in XRD were less straight-forward to identify using the SEM and EDS information. Specifically, Ca and Zr often appeared to coexist with lanthanide series elements in multiple phases making it impossible to distinguish zirconolite ($CaZrTi_2O_7$), pyrochlore ($A^{3+}{}_2Ti_2O_7$), and perovskite ($A^{2+}TiO_3$) from the composition data. It is also possible that significant elemental substitution exists in these samples making interpretation more complex. These phases are most distinctly identified in the Ca, Zr, and Nd maps. The SEM/EDS data also reveal Fe-rich and Cs-rich phases in addition to the major phases. The Fe-rich phases appear to contain Al and possibly minor amounts of Ba. This result was not unexpected considering that various parasitic phases containing Fe, Al, or Ba have been observed in previous work.[11] Furthermore, because the ceramic in this test was formulated for a pure Fe-hollandite, excess Fe would be available from its replacement by Al in the hollandite phase to from parasitic compounds. Several Cs-rich phases have also been observed in previous work. In particular, non-durable Cs-Mo containing compounds and Cs-Al titanates are known to form. Interestingly, Cs-Mo containing phases did not appear the dominant Cs-rich phase in the maps of the core samples. Instead, Cs also appeared in combination with other elements, most markedly Al and possibly various lanthanides. As noted previously, the Fe-hollandite formulation does not represent an optimal waste form composition but was selected for this initial proof-of-principal testing due to its lower melting temperature behavior and compatibility with the current INL CCIM design.

[k] Analysis excludes oxygen and elements below detection.

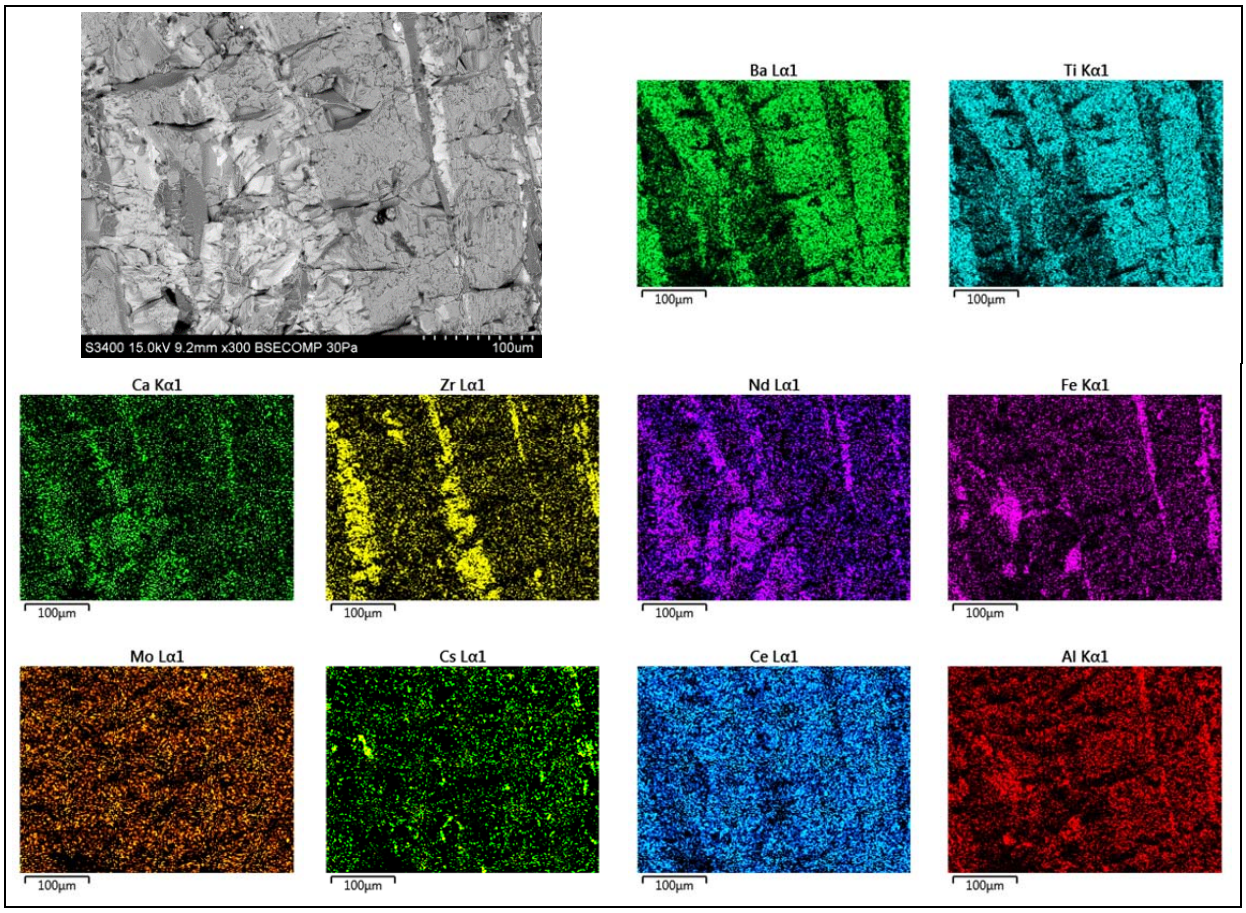

Figure 9. 300X magnification EDS elemental maps and semi-quantitative concentrations for core sample D Zone 1.

Table 5. Semi-quantitative EDS analysis of spot locations in Core D Zone 1.

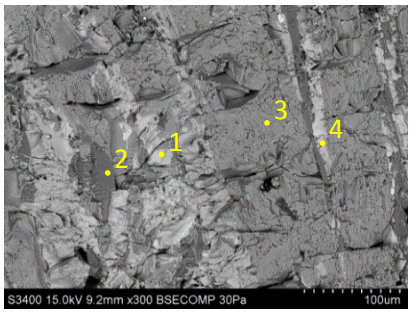

Core D Zone 1

	Spot / Atom %							
	1		2		3		4	
Ti	55.4	**Ti**	43.1	**Ti**	60.2	**Ti**	55.7
Nd	10.2	**Fe**	38.0	**Fe**	15.5	**Ca**	9.9
Ca	9.8	**Al**	15.0	**Ba**	12.0	**Fe**	9.6
Fe	8.1	**Ba**	1.5	**Al**	9.1	**Nd**	7.4
Ce	6.1	**Zr**	1.1	**Cs**	1.7	**Al**	5.9
Al	5.6	Cs	0.3	Zr	0.7	**Ce**	5.9
Ba	3.0	Nd	0.3	Ca	0.4	**Ba**	2.8
Zr	1.1	Ca	0.3	Mo	0.3	**Cs**	2.0
Cs	0.7	Ce	0.2	Nd	0.1	Zr	0.6
Mo	0.1	Mo	0.1	Ce	0.1	Mo	0.2
Possible Phase(s)	Zirconolite/ $A^{3+}/^{2+}$ Titanate	Fe-Al-Ti-O		Hollandite		$A^{3+}/^{2+}$ Titanate	

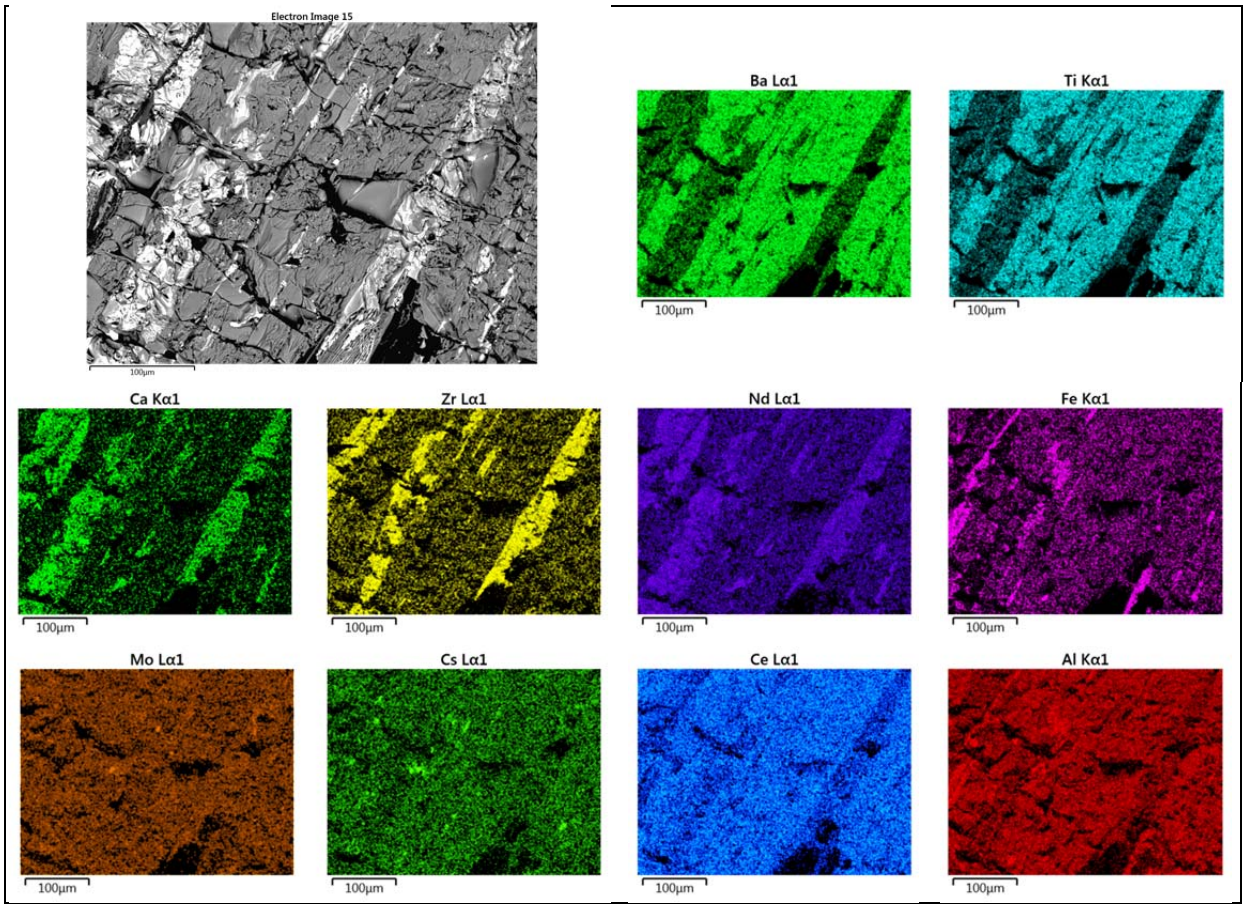

Figure 10. 300X magnification EDS elemental maps and semi-quantitative concentrations for core sample D Zone 2.

Table 6. Semi-quantitative EDS analysis of spot locations in Core D Zone 2.

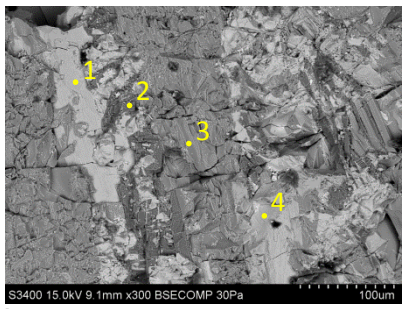

Core D Zone 2

	Spot / Atom %							
	1		2		3		4	
Ti	51.7	**Ti**	45.6	**Ti**	57.9	**Ti**	52.4
Fe	15.3	**Fe**	36.5	**Fe**	16.1	**Fe**	13.9
Zr	10.3	**Al**	13.7	**Ba**	12.4	**Zr**	10.4
Nd	7.1	**Ba**	1.6	**Al**	8.7	**Nd**	7.2
Ca	4.9	Zr	0.9	**Cs**	2.4	**Ca**	5.6
Al	4.9	Cs	0.5	**Mo**	1.2	**Al**	5.2
Ce	3.3	Nd	0.4	Zr	0.8	**Ce**	3.2
Ba	1.8	Ca	0.3	Nd	0.4	Ba	0.9
Cs	0.5	Ce	0.2	Ca	0.1	Cs	0.8
Mo	0.2	Mo	0.2	Ce	0	Mo	0.4
Possible Phase(s)	Zirconolite/ $A^{3+}/^{2+}$ Titanate	Fe-Al-Ti-O		Hollandite		Zirconolite/ $A^{3+}/^{2+}$ Titanate	

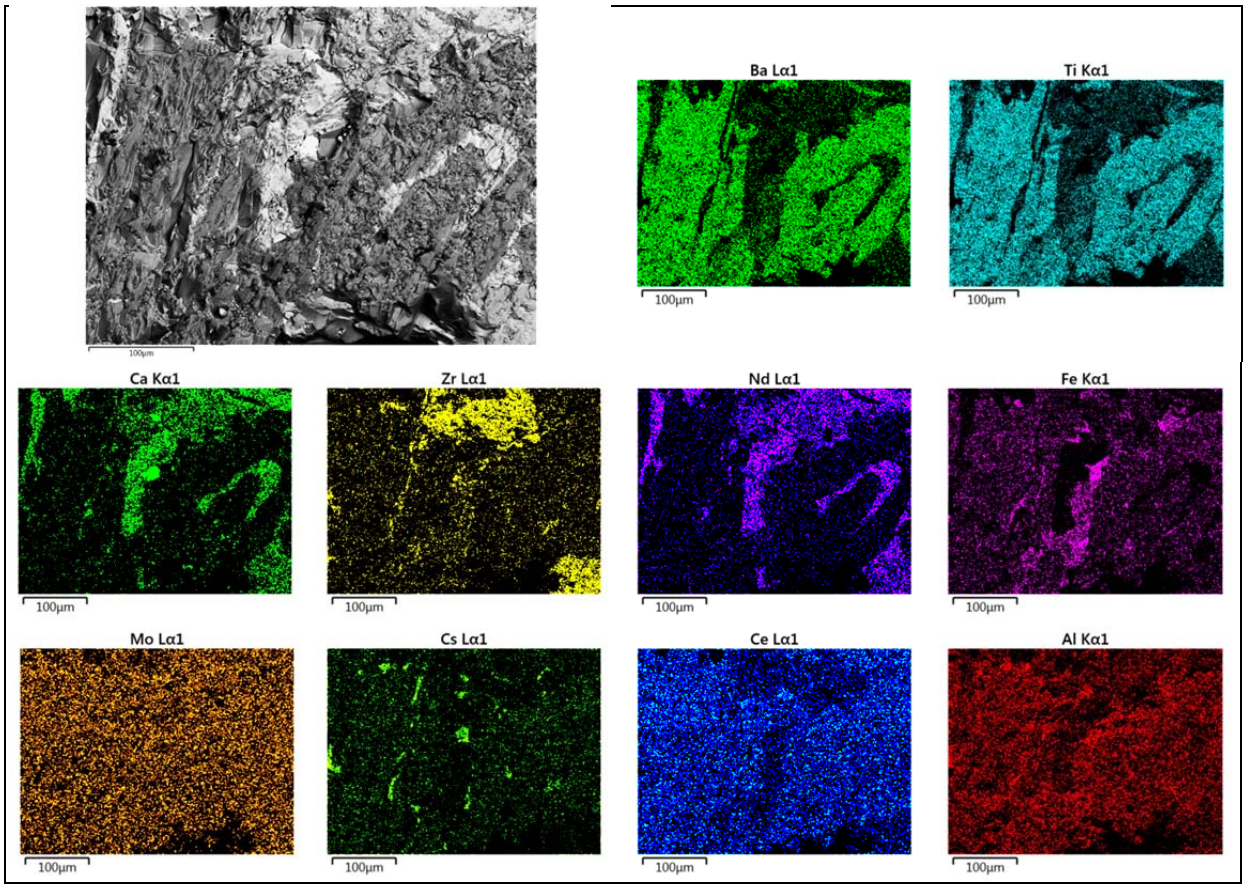

Figure 11. 300X magnification EDS elemental maps and semi-quantitative concentrations for core sample D Zone 3.

Table 7. Semi-quantitative EDS analysis of spot locations in Core D Zone 3.

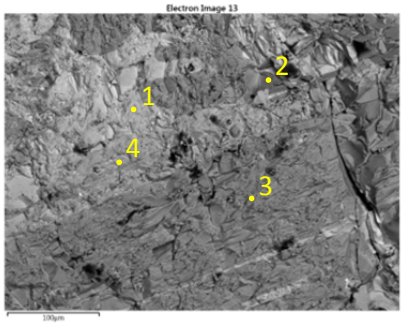

Core F Zone 1

	Spot / Atom %							
	1		2		3		4	
Ti	54.7	Ti	44.1	Ti	63.70	Ti	55.5
Nd	12.0	Fe	43.3	Fe	17.10	Fe	15.5
Ca	9.8	Al	18.0	Ba	11.40	Nd	8.7
Ce	7.5	Ba	1.0	Al	6.70	Zr	7.7
Fe	4.9	Zr	0.8	Cs	1.20	Ca	5.9
Al	3.1	Nd	0.0	Ce	0.00	Ce	4.1
Ba	2.4	Ca	0.0	Zr	0.00	Al	2.5
Zr	0.0	Ce	0.0	Mo	0.00	Ba	0.0
Cs	0.0	Cs	0.0	Ca	0.00	Cs	0.0
Mo	0.0	Mo	0.0	Nd	0.00	Mo	0.0
Possible Phase(s)	$A^{3+}/^{2+}$ Titanate		Fe-Al-Ti-O		Hollandite		Zirconolite/ $A^{3+}/^{2+}$ Titanate	

Higher magnification EDS maps of Core D Zone 1 (dense) are shown in Figure 12 that highlight the elemental partitioning in greater detail. In those maps, a Fe-Al containing phase is clearly present. Extensive mixing of Ca, Zr, Nd, and Ce suggests a high degree of elemental substitution in possibly several different phases. It is reasoned that because the ceramic is comprised of structurally similar titanate phases, elemental substitution is likely to occur in varying degrees depending on the kinetics of crystallization during processing. Cs appeared to partition to a phase(s) with Al, Zr, and other lanthanides. Notably, the Cs-rich area appears deficient of Ti and Mo suggesting previously un-identified Cs phases (i.e., Cs-Mo containing phases and Cs-Al titanate phases have been observed in previous work) were formed.

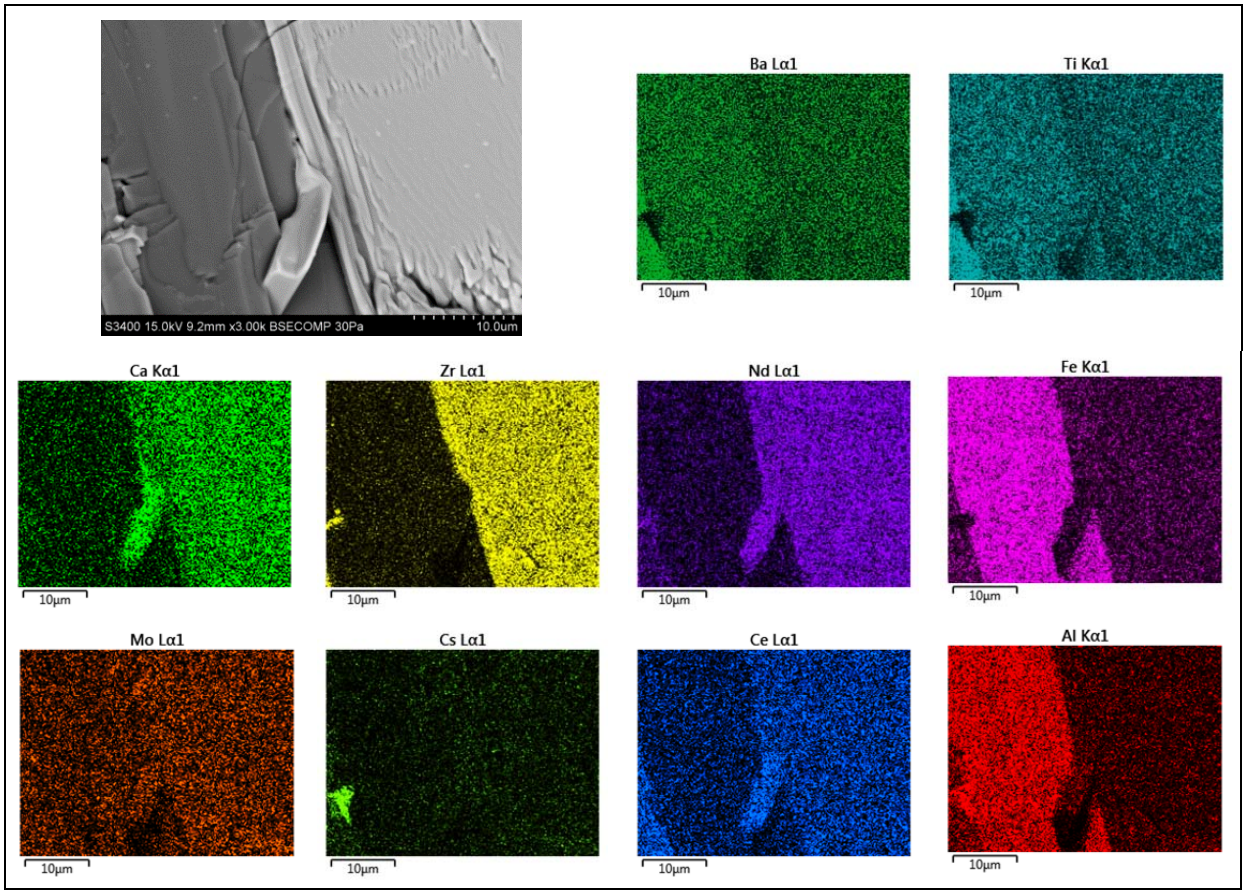

Figure 12. 3000X magnification EDS elemental maps for core sample D Zone 1.

EDS maps of Core F (near melter perimeter) are shown in Figure 13 – Figure 15 for comparison to Core D (melter center). Semi-quantitative elemental analysis was performed on several samples resulting in similar chemical makeup for the various phases. Representative EDS semi-quantitative elemental[1] compositions are shown in Table 8 – Table 10. Comparison of Core D to Core F reveals no significant differences in terms of microstructure features or phase composition/assemblage based on SEM/EDS analysis. Core E was not examined in detail as it was assumed to be similar to Core D and F, which were positioned radially on either side of Core E.

[1] Analysis excludes oxygen and elements below detection.

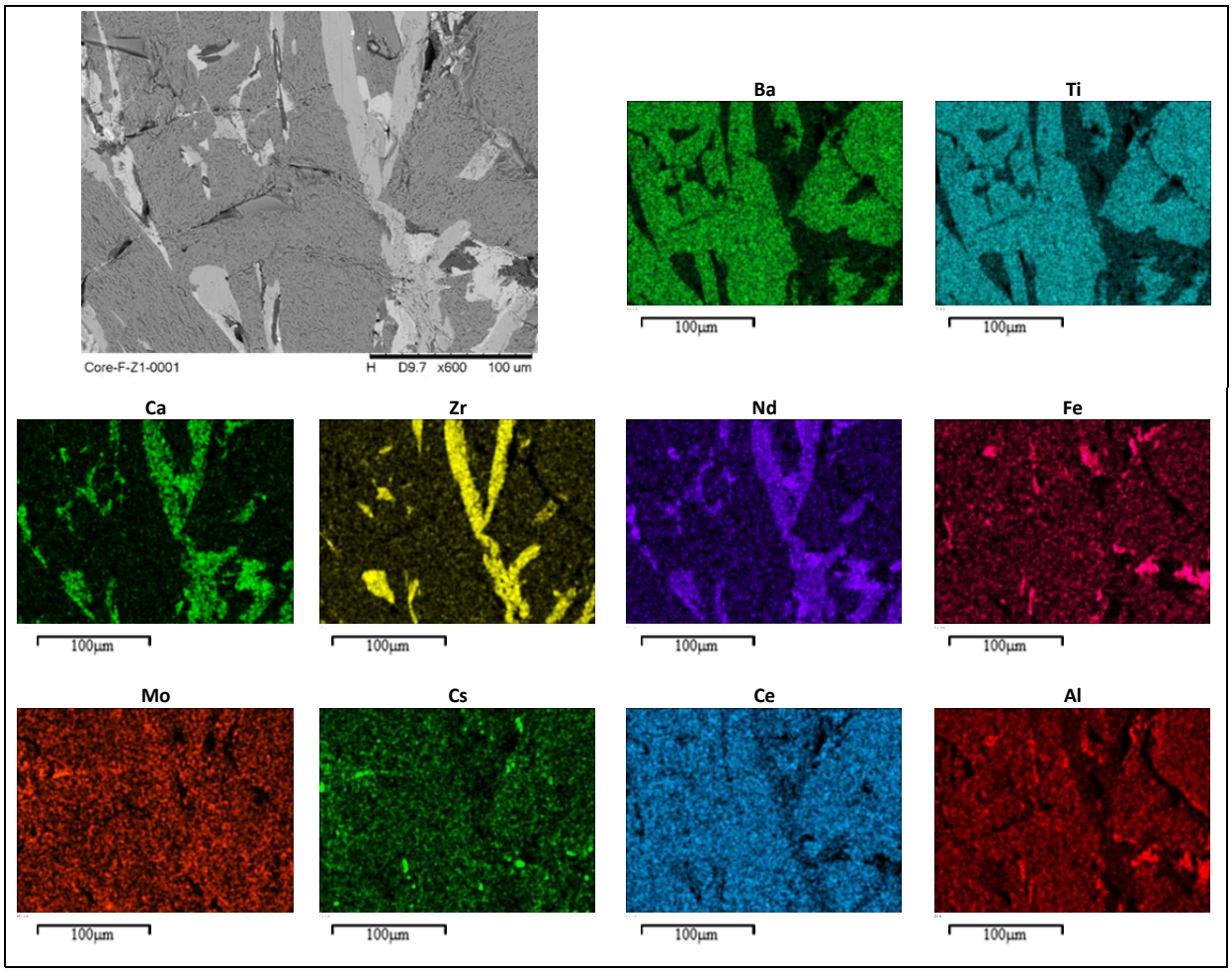

Figure 13. 600X magnification EDS elemental maps for Core F Zone 1.

Table 8. Semi-quantitative EDS analysis of spot locations in Core F Zone 1.

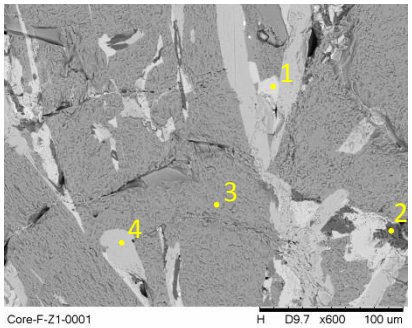

Core F Zone 1

	Spot / Atom %							
	1		2		3		4	
Ti	53.2	**Ti**	44.7	**Ti**	71.5	**Ti**	55.4
Ca	10.3	**Fe**	36.1	**Fe**	13.3	**Zr**	13.8
Nd	10.1	**Al**	16.7	**Al**	7.4	**Fe**	9.2
Ce	7.8	**Cs**	1.4	**Ba**	3.4	**Ca**	7.8
Fe	7.4	Ca	0.6	**Ce**	2.5	**Al**	5.9
Al	6.1	Mo	0.3	**Cs**	1.5	**Nd**	4.2
Cs	3.0	Ce	0.2	Zr	0.4	**Ce**	2.8
Zr	1.4	Zr	0.1	Mo	0.1	Cs	0.8
Mo	0.7	Ba	0.0	Ca	0.0	Mo	0.1
Ba	0.0	Nd	0.0	Nd	0.0	Ba	0.0
Possible Phase(s)	Zirconolite/ $A^{3+}/^{2+}$ Titanate		Fe-Al-Ti-O		Hollandite		Zirconolite/ $A^{3+}/^{2+}$ Titanate	

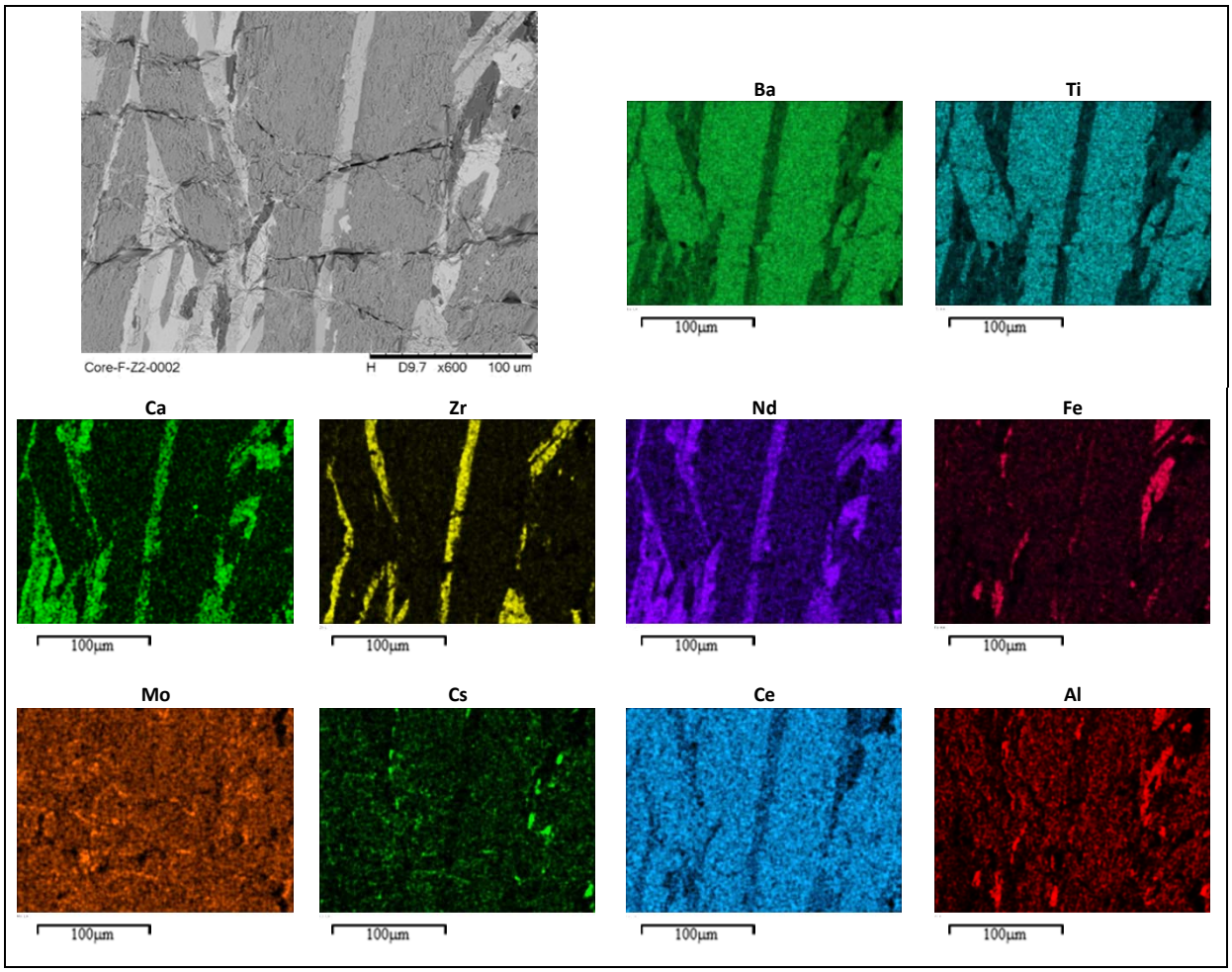

Figure 14. 600X magnification EDS elemental maps for Core F Zone 2.

Table 9. Semi-quantitative EDS analysis of spot locations in Core F Zone 2.

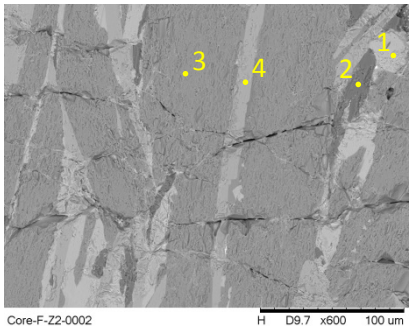

Core F Zone 2

	Spot / Atom %							
	1		2		3		4	
Ti	63.2	**Ti**	40.6	**Ti**	73.5	**Ti**	54.3
Nd	11.6	**Fe**	38.9	**Fe**	14.2	**Zr**	12.8
Ca	11.3	**Al**	14.9	**Al**	8.7	**Fe**	12.4
Fe	9.3	**Cs**	1.2	**Ba**	3.5	**Nd**	6.0
Al	7.5	Zr	0.9	**Cs**	2.2	**Ca**	5.3
Ce	7.1	Mo	0.3	**Ce**	1.8	**Al**	4.8
Cs	4.3	Ca	0.1	Mo	0.7	**Ce**	3.9
Mo	1.2	Ce	0.0	Zr	0.5	**Cs**	1.0
Zr	0.9	Ba	0.0	Ca	0.0	Mo	0.7
Ba	0.0	Nd	0.0	Nd	0.0	Ba	0.0
Possible Phase(s)	$A^{3+}/^{2+}$ Titanate	Fe-Al-Ti-O		Hollandite		Zirconolite/ $A^{3+}/^{2+}$ Titanate	

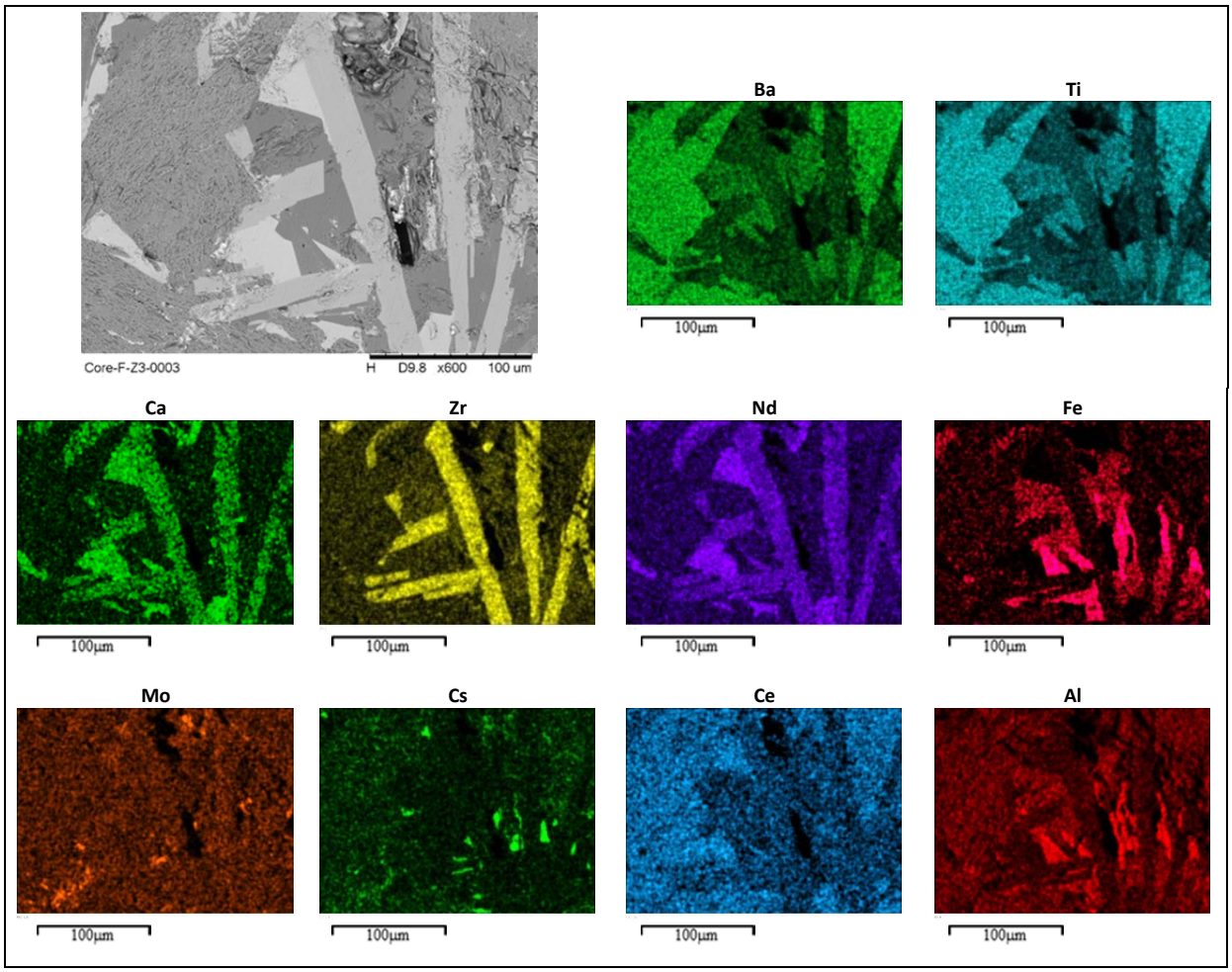

Figure 15. 600X magnification EDS elemental maps for Core F Zone 3.

Table 10. Semi-quantitative EDS analysis of spot locations in Core F Zone 3.

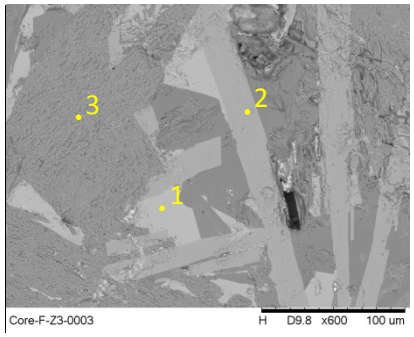

Core F Zone 3

	Spot / Atom %					
	1		2		3	
Ti	68.6	**Ti**	67.2	**Ti**	83.2
Nd	14.0	**Fe**	16.9	**Fe**	13.6
Fe	10.7	**Zr**	14.7	**Al**	9.6
Ce	10.5	**Nd**	9.4	**Ba**	3.3
Ca	9.7	**Ca**	8.1	**Cs**	3.2
Cs	4.0	**Al**	4.5	**Ce**	2.9
Al	3.2	**Ce**	3.7	Zr	0.8
Zr	0.4	**Cs**	1.4	Mo	0.6
Mo	0.0	Mo	0.1	Ca	0.2
Ba	0.0	Ba	0.0	Nd	0.0
Possible Phase(s)	$A^{3+/2+}$ Titanate		Zirconolite/ $A^{3+/2+}$ Titanate		Hollandite	

Excepting the hollandite phase, it was less straight-forward to identify phases using SEM/EDS techniques. TEM/STEM was performed on Core F Zone 1 to further investigate the chemistry and crystallinity of phases in the CCIM material. The results from TEM/STEM, EDX, and SAED are shown in Figure 16 – Figure 18. XRD, SEM, and previous understanding of the CCIM material were used in combination with EDX spectra to label the phases in Figure 16 – Figure 18. In Figure 16 the phase aligned with the electron beam was identified as zirconolite (left-hand side) with a highly crystalline structure as confirmed by the SAED pattern. The other phase was identified as hollandite (right-hand side). The interface between the two phases shown in Figure 16 (light green shaded area) is relatively sharp in the TEM image which would be expected given the structure symmetry differences between hollandite and zirconolite. The same interface between zirconolite (bottom left-hand side) and hollandite (top right-hand side) is shown in Figure 17 but with the electron beam aligned with the hollandite phase. The SAED pattern was used to confirm the crystallinity and structure of the hollandite phase. The interface between the zirconolite and hollandite phase in Figure 17 (light green shaded area) shows evidence of slight differences along the hollandite side of the interface and may indicate structural or chemical evolution along the interface. Figure 18 shows the interface between a zirconolite phase and a Fe-Al-Ti-O containing phase. The SAED pattern of the Fe-Al-Ti-O containing phase confirms it is highly crystalline. However; the Fe-Al-Ti-O containing phase could not be matched to orthorhombic or rhombohedral structures thought to exist as parasitic phases based on previous results. The interface between the two phases shown in Figure 18 (light green shaded area) is relatively sharp indicating different symmetry of the two crystalline phases.

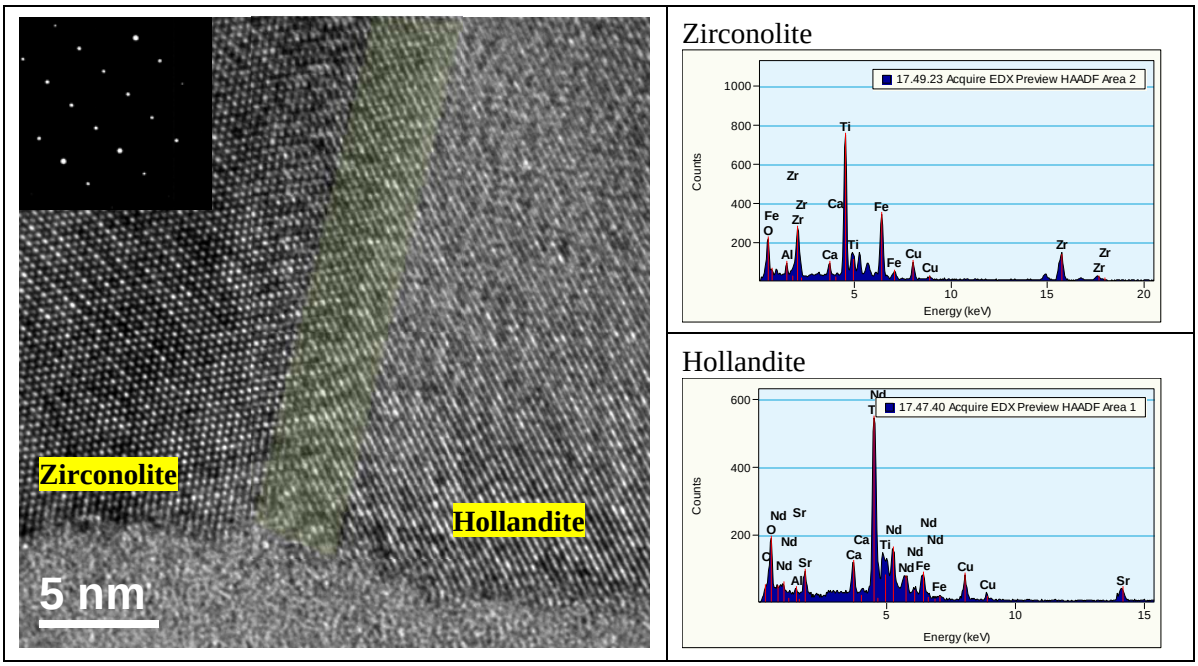

Figure 16. TEM image of hollandite and zirconolite phase interface (light green shaded area) and corresponding EDX spectra from Core F Zone 1. SAED pattern inset corresponds to the phase in which the inset is located.

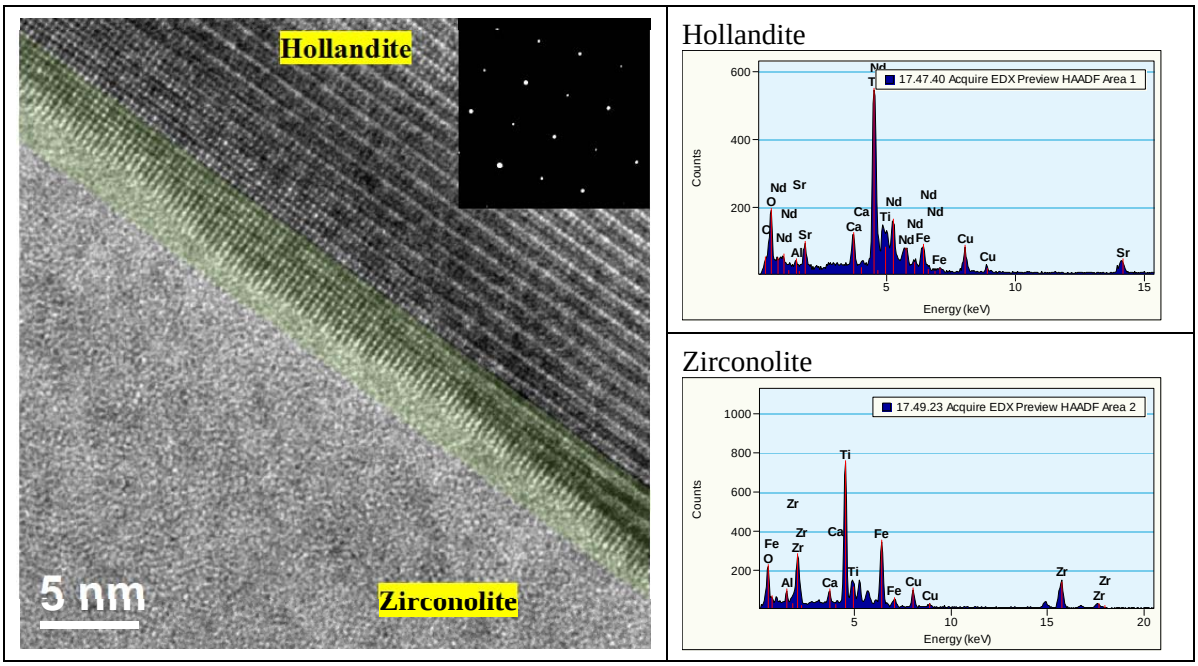

Figure 17. TEM image of hollandite and zirconolite phase interface (light green shaded area) and corresponding EDX spectra from Core F Zone 1. SAED pattern inset corresponds to the phase in which the inset is located.

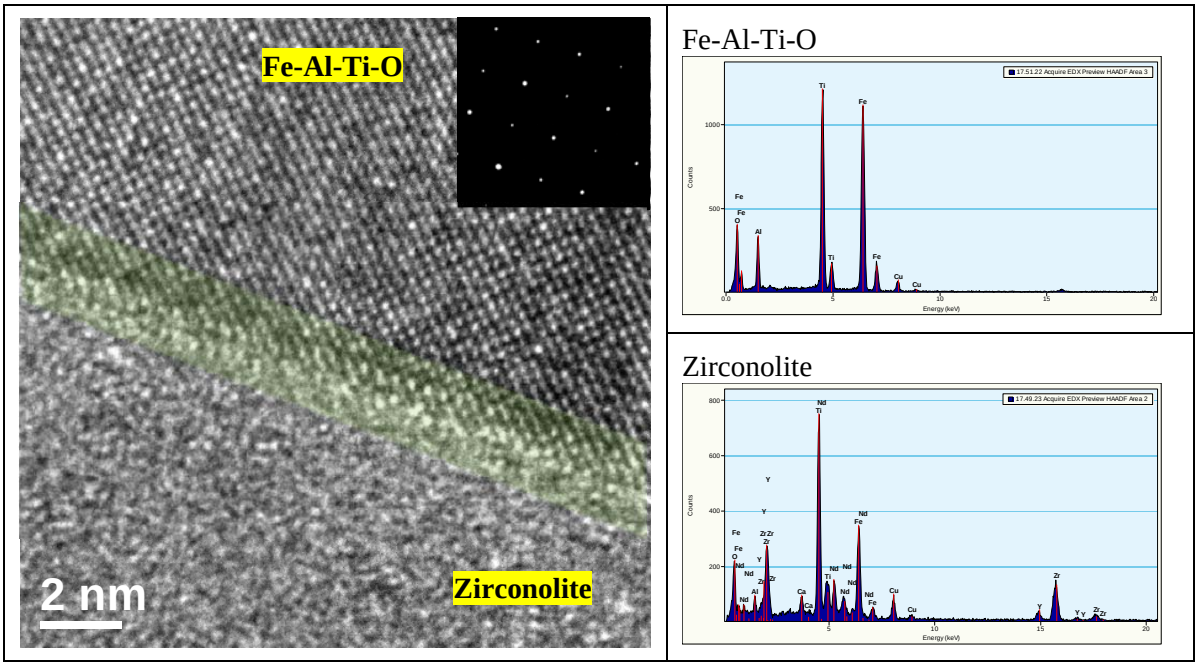

Figure 18. TEM image of Fe-Al-Ti-O and zirconolite phase interface (light green shaded area) and corresponding EDX spectra from Core F Zone 1. SAED pattern inset corresponds to the phase in which the inset is located.

3.2.4 Chemical Durability

Chemical durability was performed to assess the relative durability of different areas from the CCIM material. Specifically, potential differences in durability throughout the bulk material were tested by sampling material from different Zones (similar to the chemical composition testing). The results of the aqueous durability testing are summarized in Figure 19. Element releases not shown in Figure 19 were below detection. Similar to composition data, the greatest standard error was observed in the Zone 3 and 5 samples suggesting that precise sampling in those areas is difficult or that those areas possess a greater degree of inhomogeneity. The durability results indicate Cs and Al elemental releases were practically equivalent across all zones. The Te elemental release exhibited comparatively more variation from each zone. Additionally, Zone 1 (dense) exhibited a higher Te release compared to the other zones. Mo exhibited the greatest variation from each zone than the other elements. Recalling the SEM/EDS results, Mo appears distributed throughout the ceramic, but it would appear not well chemically incorporated into primary phases. The distribution of Te was not determined because the characteristic x-ray energy of Te is similar to Ca making it difficult to identify using EDS. Nevertheless, Te also would appear not well incorporated into the matrix phases.

Given that the Fe-MP CCIM composition was not compositionally ideal, it follows that compositional adjustment could be used to better incorporate (increase durability) of various elements. Indeed, previous work has demonstrated that is the case. Together, this most recent CCIM test and the resulting characterization and demonstrated compositional improvements support the value in a CCIM test with an improved feed composition.

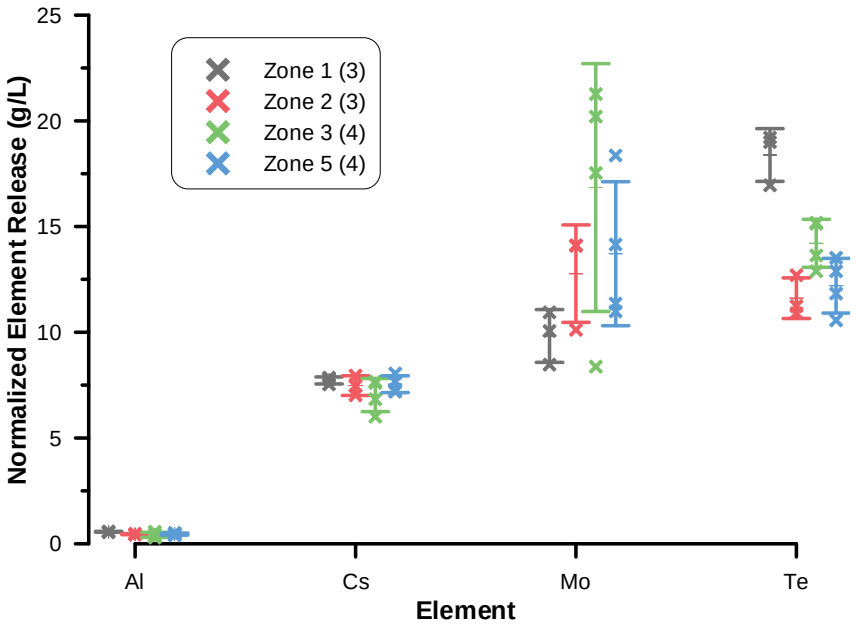

Figure 19. Normalized release for elements with measureable response after exposure to PCT. Individual samples are indicated with "x" and corresponding standard error bars are drawn.

4 DRAIN ASSEMBLY ANALYSIS

4.1 Experimental

4.1.1 Sample Preparation

The drain assembly was analyzed in order to identify why the drain heater lost power and determine if and how far material from the melt flowed into the drain. An image of the as-received drain assembly removed from the CCIM is shown in Figure 20. The drain tube was separated from the assembly and then cross-sectioned along its length using a high speed cutting saw in order to characterize the material in the drain tube. Material was recovered from 4 areas along its length (See Figure 21) and each sample was examined using XRD.[m]

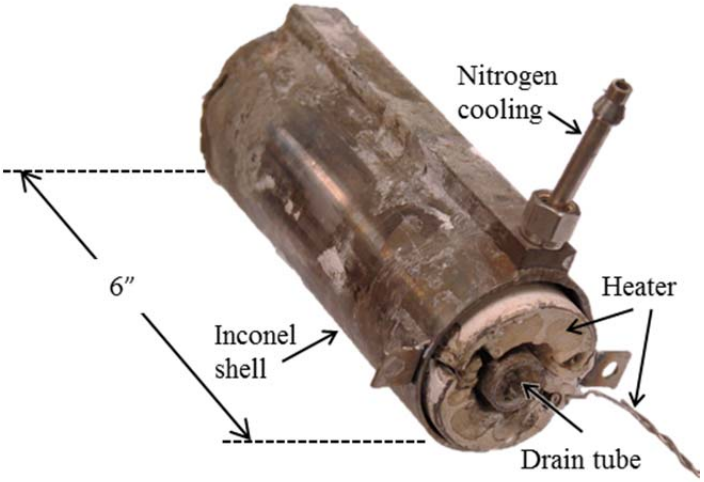

Figure 20. Drain assembly from CCIM test showing drain tube.

4.2 Results & Discussion

Prior to initiating the CCIM test, a low-temperature melting phosphate glass was used as a plug to prevent uncontrolled draining during melter initiation and heat up.[13] Figure 21 is an image of the drain tube halves after sectioning. In that image, a mixture of different material is evident as well as void space. The mixture of materials was not unexpected considering a phosphate plug was utilized during the test. As Fe was the only common component between the phosphate plug and the ceramic surrogate compositions, XRD analysis was expected to be sufficient to distinguish between ceramic surrogate material and original phosphate glass plug material. The XRD results are summarized in Table 11.

XRD analysis confirmed material in the top portion of the drain tube was identical to that in the core samples (i.e. material from the melt partially filled the drain). Furthermore, zirconolite was identified in material 2/3 – 3/4 (~4 – 5 inches) the distance from the top of the drain tube indicating ceramic surrogate material nearly exited the drain tube. Phosphate- and silicate- containing phases were found in that material as well indicating a mixture of ceramic surrogate and phosphaste glass plug material. At the bottom most ½ inch of the drain tube, XRD identified phosphate plug material without evidence of ceramic surrogate material. In addition to phase identification, the XRD patterns in

[m] Refer to Section 3.1.4 for XRD experimental parameters.

Table 11 reveal increasing glassy phase concentration in the drain tube material from top to bottom, confirming that ceramic surrogate material traveled well into the drain tube and intermixed with the phosphate plug material.

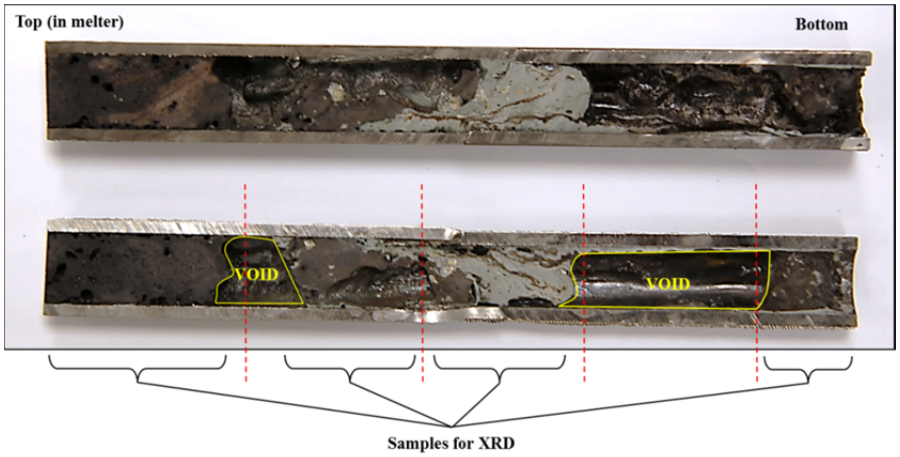

Figure 21. Cross-sections of drain tube. Sections of material analyzed for phase identification and void spaces are labeled on the bottom image.

Table 11. Summary of XRD analysis of material removed from the drain tube.

Source	XRD Patterns	Possible Phases (<PDF #>)
	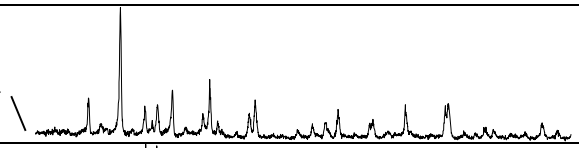	$Ba_{1.143}Fe_{2.286}Ti_{5.714}O_{16}$ <00-051-1900> $CaZrTi_2O_7$ <00-034-0167> $La_{0.4}Ca_{0.4}TiO_3$ <00-055-0841>
	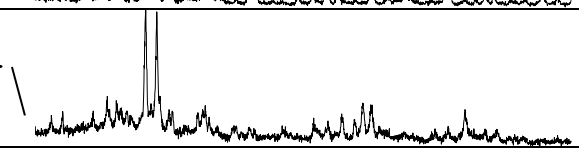	$CaZrTi_2O_7$ <00-034-0167> $LiNdSiO_4$ <00-048-0007> $(La,Ce)PO_4$ <00-054-0021> $Ca_3(PO_4)_3F$ <00-050-1306> $Gd_2Ti_2O_7$ <00-023-0259>
	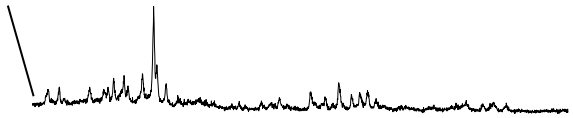	$CaZrTi_2O_7$ <00-034-0167> $LiNdSiO_4$ <00-048-0007> $(La,Ce)PO_4$ <00-054-0021> $Ca_3(PO_4)_3F$ <00-050-1306>
	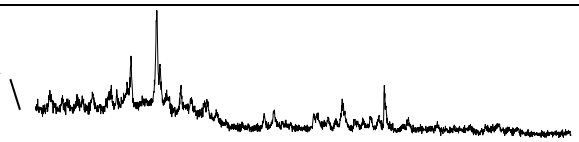	$(La,Ce)PO_4$ <00-054-0021> $Ca_3(PO_4)_3F$ <00-050-1306> Cr_2O_3 <00-038-1479>
	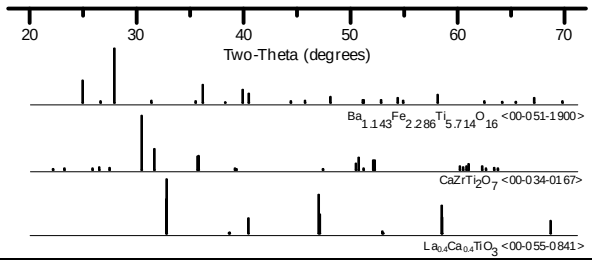	

5 CONCLUSIONS

The first scaled proof of principle test for processing multi-phase crystalline waste forms from a melt was completed using the CCIM at INL in October 2014. During this initial test, although the drain operation could not be completed, a ceramic was fabricated from a melt process for treating the HLW stream generated from an envisioned commercial spent nuclear fuel reprocessing flow sheet. Characterization of material produced during the test indicated that the ceramic material exhibited a desirable phase assemblage consisting primarily of hollandite, zirconolite, and pyrochlore/perovskite phases. Characterization performed throughout various locations (both vertically and radially) in the processed material confirmed that the ceramic material was compositionally homogenous. Similarly, durability testing indicated the material was homogeneous. This recent CCIM test and the resulting characterization in conjunction with demonstrated compositional improvements provide justification for future melt-processed ceramic waste form testing.

Additional outcomes from this initial test are an increased understanding of the capabilities of the INL CCIM including the drain and power systems while operating at previously unattained temperatures. Information from analyzing the drain assembly and operation parameters has been used to re-design a crucible and drain system for the melter to support future testing. Additionally, although the CCIM was able to sustain a melt at temperature in excess of 1500°C, the power supply was operating at its limits. It is recommended that a power system with greater variation in frequency and total power be acquired to expand the versatility and capabilities of the CCIM at INL.

6 REFERENCES

1. D. S. D. Gunn, N. L. Allan, H. Foxhall, J. H. Harding, J. A. Purton, W. Smith, M. J. Stein, I. T. Todorov and K. P. Travis, "Novel Potentials for Modelling Defect Formation and Oxygen Vacancy Migration in $Gd_2Ti_2O_7$ and $Gd_2Zr_2O_7$ Pyrochlores," *Journal of Materials Chemistry*, **22** [11] pp. 4675-4680, (2012).

2. R. Ubic, I. M. Reaney and W. E. Lee, "Perovskite $NdTiO_3$ in Sr- and Ca-doped BaO-Nd_2O_3-TiO_2 Microwave Dielectric Ceramics," *Journal of Materials Research*, **14** [04] pp. 1576-1580, (1999).

3. H. F. Xu and Y. F. Wang, "Crystallization Sequence and Microstructure Evolution of Synroc Samples Crystallized from $CaZrTi_2O_7$ Melts," *Journal of Nuclear Materials*, **279** [1] pp. 100-106, (2000).

4. V. Aubin-Chevaldonnet, D. Caurant, A. Dannoux, D. Gourier, T. Charpentier, L. Mazerolles and T. Advocat, "Preparation and Characterization of $(Ba,Cs)(M,Ti)_8O_{16}$ ($M = Al^{3+}$, Fe^{3+}, Ga^{3+}, Cr^{3+}, Sc^{3+}, Mg^{2+}) Hollandite Ceramics Developed for Radioactive Cesium Immmobilization," *Journal of Nuclear Materials*, **366** [1-2] pp. 137-160, (2007).

5. M. L. Carter, E. R. Vance and H. Li, "Hollandite-rich Ceramic Melts for Immobilization of Cs," *Mat. Res. Soc. Symp. Proc.*, **807** pp. 249-254, (2003).

6. M. L. Carter, E. R. Vance, D. R. G. Mitchell and Z. Zhang, "Mn Oxidation States in $Ba_xCs_yMn_zTi_{8-z}O_{16}$," *Mat. Res. Soc. Symp. Proc.*, **824** pp. CC4.6.1 - 6, (2004).

7. J. W. Amoroso and J. C. Marra, "Ceramic Waste Form Data Package: Fuel Cycle Research and Development," *US Department of Energy Report Office of Nuclear Energy Separations and Waste Forms Campaign SRNL-STI-2014-00247 (FCRD-SWF-2014-000581)*, Savannah River National Laboratory, Aiken SC (2014).

8. E. W. Baumann, "Colorimetric Determination of Ferrous-Ferric Ratio in Glass," *US Department of Energy Report DPST-87-304, DPST-87-304*, Savannah River Laboratory, Aiken (1987).

9. C. M. Jantzen, "Characterization of the Defense Waste Processing Facility (DWPF) Enviornmental Assessment (EA) Glass Standard Reference Material," *Westinghouse Savannah River Company Technical Report*, pp. (1993).

10. *Standard Test Methods for Determining Chemical Durability of Nuclear, Hazardous, and Mixed Waste Glasses and Multiphase Glass Ceramics: The Product Consistency Test (PCT), 2002*, pp.

11. J. Amoroso, J. Marra, S. D. Conradson, M. Tang and K. Brinkman, "Melt Processed Single Phase Hollandite Waste Forms for Nuclear Waste Immobilization: Ba1.0Cs0.3A2.3Ti5.7O16; A = Cr, Fe, Al," *J. Alloys Compd.*, **584** pp. 590-99, (2014).

12. K. Brinkman, J. Amoroso, J. Marra and M. Tang, "Crystalline Ceramic Waste Forms: Comparison of Reference Process for Ceramic Waste Form Fabrication," *US Department of Energy Report SRNL-STI-2013-00442 (FCRD-SWF-2013-000229)*, Savannah River National Laboratory, Aiken SC (2013).

13. V. C. Maio, "Production of a Low Temperature SYNROC All Ceramic Surrogate High Level Waste Form in INL's Cold Crucible Induction Melter Pilot –Validation of Test Completion," *U.S. Department of Energy Report INL/MIS-14-34012 (FCRD-SWF-2015-00256)*, Idaho National Laboratory, Idaho Falls, ID (2014).